ELSEVIER

Nuclear Instruments and Methods in Physics Research B 187 (2002) 492–498

NIM B
Beam Interactions with Materials & Atoms

www.elsevier.com/locate/nimb

Incidence characteristics of alpha particles on detectors irradiated in a radon + progeny atmosphere

D. Nikezic [1], K.N. Yu *

Department of Physics and Materials Science, City University of Hong Kong, Tat Chee Avenue, Kowloon Tong, Kowloon, Hong Kong

Received 30 August 2001; received in revised form 27 October 2001

Abstract

The angular and energetic distribution of alpha particles from the ^{222}Rn chain in air incident on a detector have been determined by the Monte Carlo method. Stopping power of alpha particles in air have been taken from the ICRU49 report. The incident alpha-particle spectrum was found for various equilibrium factors. It has been shown that the spectrum between 5.5 and 7.69 MeV depends on the equilibrium factor. High resolution alpha spectrometry can enable the measurements of concentrations of ^{214}Po and ^{218}Po in air. The maximal sensitivity coefficient has also been determined for measurements of ^{214}Po concentrations.

PACS: 29.40; 23.60
Keywords: Natural radioactivity; Radon; Detector sensitivity; Monte Carlo methods

1. Introduction

It has been established a long time ago that the absorbed radon dose in the human lung is not delivered by radon itself, but instead mostly caused by its short-lived progeny. The absorbed dose is commonly determined by first measuring the radon concentration and then applying an assumed equilibrium factor between radon and its progeny (usually about 0.5). This forms the base for determining the *exposure* to radon progeny expressed in the traditional unit working level month (WLM). The exposure can then be multiplied with the dose conversion coefficient, which is nominally recommended to be 5 mSv/WLM, to give the effective dose [1]. A drawback for these procedures is the requirement to assume a equilibrium factor. Until now, there is no widely accepted methods for long-term passive measurements of radon progeny concentrations, despite that short-term active measurements are relatively easy by air filtering and subsequent activity measurements on the filter. For this reason, exploration of long-term passive integration measurement methodologies regarding short-lived radon progeny has attracted much attention in the field of radon dosimetry.

* Corresponding author. Tel.: +852-2788-7812; fax: +852-2788-7830.
E-mail address: peter.yu@cityu.edu.hk (K.N. Yu).
[1] On leave from Faculty of Sciences, University of Kragujevac, 34000 Kragujevac, Yugoslavia.

0168-583X/02/$ - see front matter
PII: S0168-583X(01)01146-6

There are a few different approaches to this problem, all of them being based on the usage of solid state nuclear track detectors (SSNTDs). Here, we should mention the double detector method, in which one detector is placed in a diffusion cup (measuring only radon) and another one is open (or bared, measuring radon + progeny). The ratio k of these track densities, namely ρ_{open} and ρ_{cup}, respectively, i.e., $k = \rho_{\text{open}}/\rho_{\text{cup}}$, is related to the equilibrium factor F. Although this method is easy to apply, it was shown [2] to be rather inaccurate because the function $F(k)$ is too steep. One of the directions nowadays is to exploit alpha spectroscopy [3], also with SSNTDs, while another one is to explore particular etching conditions in such a way that only tracks with specified characteristics or in particular energy windows are seen on the detector [4].

The present paper is devoted to studying the incidence characteristics of alpha particle, viz., the energetic distribution (i.e., the alpha-particle spectrum) and angular distribution of the alpha particles entering the detector. These results are in fact not restricted to SSNTDs, but are valid for all types of detectors.

2. Determination of angular and energetic distribution of incident particles

The incident spectrum of alpha particles depends on the equilibrium factor, F, between radon and its progeny. This dependence will be examined and quantified here. It will be necessary to establish the incident spectrum of the particles on the detector for a given exposure condition. Although the problem seems trivial, to the best of our knowledge, this has not been clearly documented in the literature. Determination of these distributions was carried out using the Monte Carlo method. The geometry of the problem is shown in Fig. 1.

Below the theoretical critical angle, θ_c, no detection is possible. In the following calculations, the critical angle for CR39 detector is used, but the calculations can be easily extended to other types of detectors. The theoretical critical angle of the CR39 detector is determined by the equation

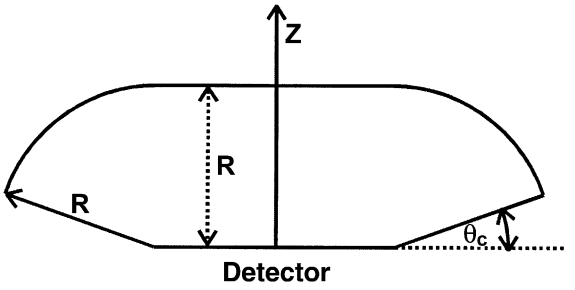

Fig. 1. The geometry used for determining the angular and energetic distribution of the particles incident on the detector. R is the range of alpha particles and θ_c is the theoretical critical angle for a given detector. The center of the detector is adopted as the origin of our coordinate system. The three dimensional image is obtained by rotation of the curve in this figure.

$$\theta_c = \arcsin\frac{1}{V_0}, \tag{1}$$

where V_0 is the maximal value of the ratio V_t/V_b, V_t is the track etch rate (i.e., the etch rate along the track) and V_b the bulk etch rate. The function $V_t(R')$ was chosen for this detector, where R' was the residual range. There are a few different functions proposed for V_t/V_b in the literature, and we here adopt the one given in [5], i.e.,

$$V = 1 + \left(11.45e^{-0.339R'} + 4e^{-0.044R'}\right)\left(1 - e^{-0.58R'}\right). \tag{2}$$

The maximal value of this function, which is equal to 7.5, is obtained for the residual range of 2.2 μm. Therefore the theoretical critical angle is $\theta_c = \arcsin(1/7.53) = 7.63°$. No tracks can be formed below this angle for any incident energy. It is also noted that the calculations presented below are not very sensitive to the value of θ_c.

A three dimensional image is obtained by rotation of the curve in Fig. 1 around the z-axis, assuming that the detector is circular in shape. Starting points of alpha particles for Monte Carlo simulations are chosen randomly inside the frame shown in Fig 1. Such a sampling reflects the assumption of a uniform distribution of radon and progeny within the air. Determination of the energy distribution requires a knowledge of the path length distribution $f(x)$ for the particles that eventually hit the detector. $f(x)\,dx$ is then the

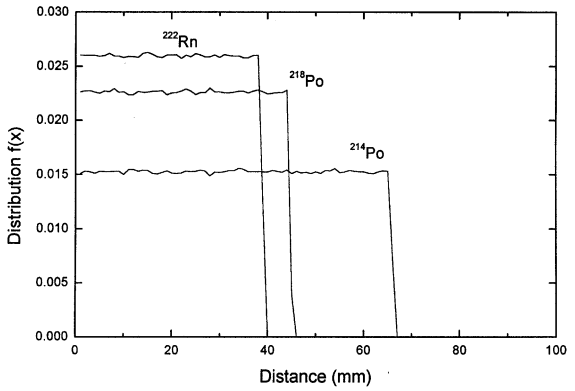

Fig. 2. Path length distribution for ^{222}Rn, ^{218}Po and ^{214}Po with emission energies of 5.49, 6 and 7.69 MeV, respectively.

probability that the particle travels a distance from x to $x + \mathrm{d}x$ before it hits the detector. The path length distributions for emission energies E_0 of 5.49, 6 and 7.69 MeV are given in Fig. 2.

Simulations were performed with 10^6 particles that hit the detector for each of the three emission energies. The path length is the distance between the starting point and the point where the particle enters the detector surface. The y-axis in Fig. 2 denoted by $f(x)$ is the probability that the particle travels the distance between x and $(x+1)$ mm before it strikes the detector. Since the selected step size was 1 mm, the curves in Fig. 2 can also be considered as a probability density distribution.

These distribution have to be transformed to energy distributions. The stopping power of alpha particles in air is needed for this task. The stopping power, $S(E)$, for the alpha particles in dry air at sea level was adopted form the ICRU49 report [6]. In the report, stopping power was given as a function of alpha particle energy. However, in our calculations, the residual energy E after traveling the distance l, i.e., $E(l)$, is needed for the emission alpha particles energy E_0. Determination of the function $E(l)$ was carried out as follows. First, the data given for the linear stopping power of alpha particle in air were fitted by the function

$$-\frac{\mathrm{d}E}{\mathrm{d}x} = S(E) = \sum_{i=1}^{5} a_i E^{b_i} \mathrm{e}^{c_i E}, \tag{3}$$

which gave the coefficients

$$a_1 = -14.42; \quad a_2 = 17.05; \quad a_3 = 207.4;$$
$$a_4 = -87.89; \quad a_5 = -130.5; \quad b_1 = 0.4301;$$
$$b_2 = 0.3222; \quad b_3 = 0.5947; \quad b_4 = 0.7725;$$
$$b_5 = 0.5118; \quad c_1 = -0.2149; \quad c_2 = -0.1945;$$
$$c_3 = -2.136; \quad c_4 = -2.040; \quad c_5 = -2.308.$$

Errors introduced by the fit was found to be less than 1% in the region of interest ($E < 7.69$ MeV). The energy of an alpha particle after traversing a distance x in the air can be determined as follows. From the previous equation one can find

$$-\frac{\mathrm{d}E}{S(E)} = \mathrm{d}x, \tag{4}$$

which gives on integration

$$\int_{E_1}^{E_0} \frac{\mathrm{d}E}{S(E)} = \int_{E_1}^{E_0} \frac{\mathrm{d}E}{\sum_{i=1}^{5} a_i E^{b_i} \mathrm{e}^{c_i E}} = \int_0^1 \mathrm{d}x = l, \tag{5}$$

where E_0 is the emission energy of the alpha particle and E_l its energy after traversing the distance l in air. The function $E(l)$, i.e., the energy of the alpha particle after traversing the distance l in air, was tabulated from the previous equation. This has been repeated for all three alpha energies in the ^{222}Rn chain, with distance steps of 0.1 mm. For l values in between the tabulated values, linear interpolation was employed. These tables have been used to establish the incident alpha-energy spectra, and the results are shown in Fig 3.

These distributions are in fact distorted path length distributions, because the alpha particles do not lose energy uniformly along their paths. The values on the y-axis give the probability $f(E)$ that the alpha particle energy incident on the detector is in the interval $(E, E + 0.1)$ MeV. Calculations were performed with 10^6 incident particles.

Beside the energetic distribution, the angular distribution of incident particles is also needed for some kind of detectors. For example, in SSNTDs, the incident angle is one of the factors that determine the track parameters. The angular distribution of incident particles is also calculated by the Monte Carlo method as before. The results are presented in Fig. 4. Here, the y-axis $f(\theta)$ gives the probability for the particle with an incident angle

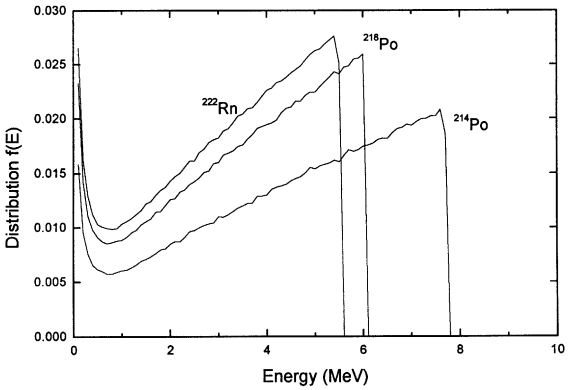

Fig. 3. Incident energy distribution for three alpha particle energies in the ^{222}Rn chain.

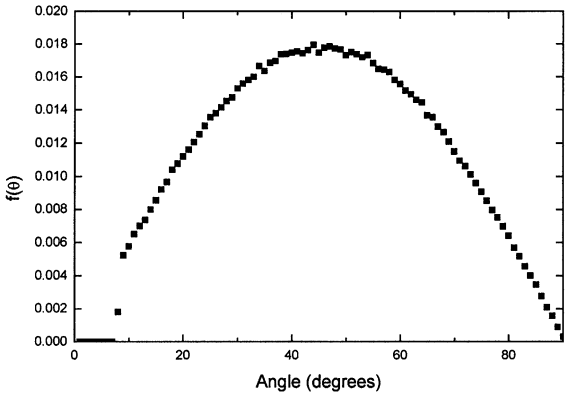

Fig. 4. Angular distribution of incident particles.

between $\theta°$ and $(\theta+1)°$, and can also be considered as a probability density distribution.

Although the particles are emitted isotropically, the distribution in Fig. 4 is not uniform. The maximum of the distribution is about 45°. The lowest part of the distribution is cut at the theoretical critical angle θ_c. The shape of the distribution shown in Fig. 4 is the result of the complicated interplay between the distance, the angle subtended by the detector as seen from the emission point and the isotropic emission of alpha particles.

These results can be easily understood by inspecting Fig. 5. If an alpha particle is emitted at point A, the probability for it to strike the detector perpendicularly is proportional to the small area around A′ which is the vertical projection of point

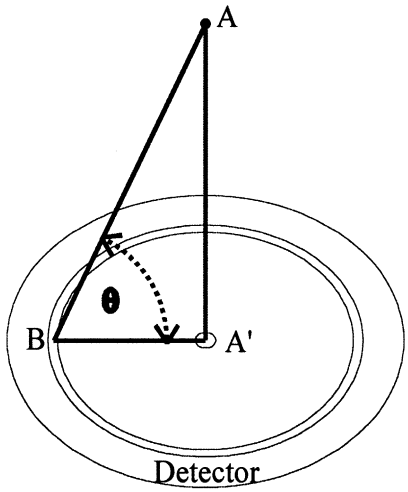

Fig. 5. Explanation of the graph in Fig. 4.

A onto the detector plane. However, the probability for the alpha particle to strike the detector with angle θ is proportional to the surface area of the infinitesimal ring around the point A′ with θ as the angle between any point in the ring and point A (see Fig. 5). The area in this ring is much larger than the previous small area around A′.

The angular distribution does not depend on the incident alpha particle energy. The results for all alpha energies in the radon chain have been obtained in the present work, but they are essentially the same, so only one group of the results is shown here. One can see from Fig. 4 that the number of particles striking the detector perpendicularly (90°) should be very small. Some radon progeny measurements are based on measuring circular tracks in solid state nuclear track detectors (SSNTDs), which originate from normal incidence. Due to the relatively small number of such particles, the counting statistics can be poor and the uncertainty can be large.

The curve in Fig. 4 is of general importance for all kinds of detectors exposed to radon and progeny. All distributions given above have been obtained using 10^6 particles which have hit the detector. The number of particles in an energy interval or an angle interval is then divided by 10^6 to give the probability of a particle entering the detector from that particular interval. The next

step is to transform these distributions (energy and angular distributions) for a realistic detector exposure to radon and its short-lived progeny, and energy and angular distributions are obtained for a given exposure condition. To perform such recalculations, the quantity here called the hit efficiency, ε_{hit}, should be used, which is the ratio of the number of particles that hit the detector and the total number of particles emitted in the volume V with a distance R from the detector (Fig. 1). This quantity is also determined by the Monte Carlo method.

The number of hits, N_{hit}, is given by

$$N_{\text{hit}} = \varepsilon_{\text{hit}} AVt, \tag{6}$$

where A is the assumed activity of an alpha emitter in air (in Bq m^{-3}), V the volume (in m^3) and t (in s) the duration of irradiation. We assumed the radon activity A_0 to be 1 Bq m^{-3} and the activity of its progeny ^{218}Po, ^{214}Pb and ^{214}Bi/Po to be F_1A_0, F_2A_0 and F_3A_0, respectively (F_i are the activity ratios of radon progeny to radon). The values for ε and V are given in Table 1.

The incident alpha-particle spectrum for mixed (radon + progeny), which is always the case in nature, is obtained by summing up the distributions presented in Fig. 3, weighted by the relative number of hits by the respective progeny. The results are shown in Fig. 6.

In Fig. 6, the y-axis gives the fraction of particles with energy in the interval $(E, E + 0.1$ MeV) incident on the detector. The curves apply in general to all detectors irradiated by radon and progeny in air. Similar curves were given by Baixeras et al. [4] but were presented with *arbitrary units*.

The results in Fig. 6 are given for two extreme cases, namely, for an equilibrium factor $F = 1$ and for a low equilibrium factor $F = 0.1$. The curves in Fig. 6 show a non-Gaussian peak at 5.49 MeV and cutoff structures above 5.49 MeV. The first cutoff

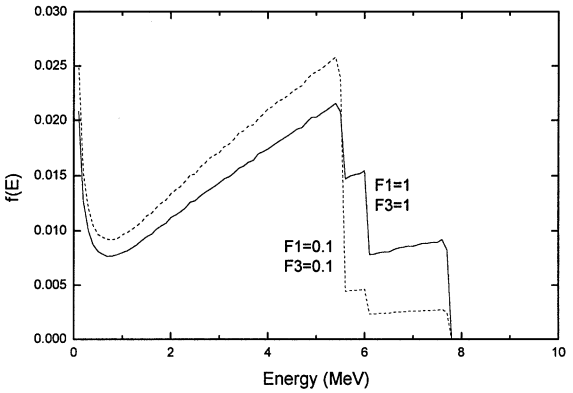

Fig. 6. Incident alpha-particle spectrum for mixed (radon + progeny).

from right to left is related to ^{214}Po while the second to ^{218}Po. The curves have plateaus between 6 and 7.69 MeV and between 5.69 and 6 MeV; the former (^{214}Po plateau) is wider because of the wider energy gap, while the latter (^{218}Po plateau) is narrower and higher than the ^{214}Po plateau. By analyzing the height of these two plateaus, we can infer some information about the relative activities of ^{218}Po and ^{214}Po. If their activities are equal (as shown in Fig. 6 where $F_1 = F_3$), the ^{218}Po plateau is two times higher than the ^{214}Po plateau.

The process of plateout will create two peaks at 6 and 7.69 MeV in the measured spectrum. The heights of these peaks depend on the amount of plateout as well as the detection efficiency of the detector and the measuring conditions. The most important part of the spectrum is between 6 and 7.69 MeV. Here, only ^{214}Po from air contributes to the detector response. In order to avoid the influence of plateout (if SSNTDs are considered), the energy window between 6.2 and 7.5 should be considered. Actually the width of the window depends on the energy resolution attainable in measurements, but of course, it should not be wider

Table 1
Hit efficiency in the interval between 6.2 and 7.5 MeV, and effective volumes for alpha particles emitted in the ^{222}Rn chain

Radionuclide	Hit efficiency (ε)	Hit efficiency ($\varepsilon_{\text{interval 6.2–7.5 MeV}}$)	Effective volume (cm^3)
^{222}Rn	0.01681	–	182.53
^{218}Po	0.01309	–	258.558
^{214}Po	0.006965	0.001748	723.98

than the range from 6 to 7.69 MeV. If the energy resolution is worse than 1 MeV, measurements of radon progeny would not be possible by analyzing the energy spectrum. Feasibility of radon progeny measurement relies on the provision of high resolution alpha spectroscopy.

2.1. Number of hits between 6.2 and 7.5 MeV

In the course of simulation, the number of particles between 6.2 and 7.5 MeV was recorded, which was divided by the total number of simulations (being equal to the number of emitted particles) at the end to give the hit efficiency $\varepsilon_{\text{interval}}$ in this energy interval. The results for $\varepsilon_{\text{interval}}$ are also given in Table 1. The equation

$$N_{\text{hit,interval}} = \varepsilon_{\text{interval}} AVt \tag{7}$$

gives the number of hits in the considered energy interval. If we choose $A = 1$ Bq m^{-3} and $t = 1$ s, we have

$$\begin{aligned} N_{\text{hit,interval}} &= 1.748 \times 10^{-3} \times 1(\text{Bq m}^{-3}) \times 1(\text{s}) \\ &\quad \times 723.98 \times 10^{-6}\ \text{m}^3 \\ &= 1.26 \times 10^{-6}\ (\text{hits per 1 Bq s m}^{-3}). \end{aligned}$$

This is the sensitivity of a detector for ^{214}Po measurements (with critical angle as given before) assuming it registers all particles with energy between 6.2 and 7.5 MeV striking it. The angular distribution of this important group of particles is the same as that given in Fig. 4. This has been verified but the results are just the same as those in Fig. 4. and will not be reproduced here. The detector response to this group of particles can be derived from the value given above by taking into account the angular dependence of a particular type of detector and the angular distribution of the incident particles.

In Fig. 7, the alpha spectrum between 5 and 8 MeV is shown for three different equilibrium factors. The curves for $F = 1$ and $F = 0.1$ are the same as those in Fig. 6, and the newly added one is for $F = 0.366$, which is obtained using $F_1 = 0.8$, $F_2 = 0.4$ and $F_3 = 0.2$ representing a realistic situation. This figure demonstrates that the altitude of the plateau depends on the ratio F_1/F_3. We denote

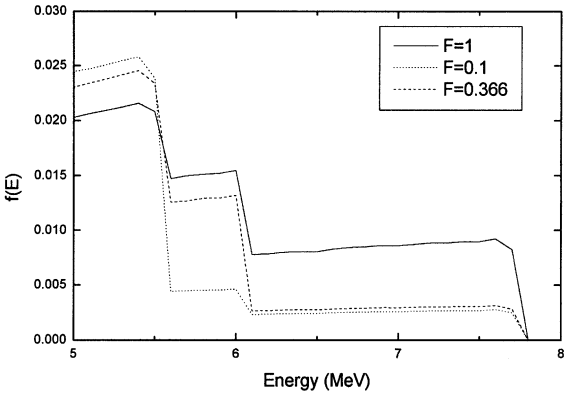

Fig. 7. Incident alpha-particle spectrum for various equilibrium factors.

the heights of the ^{214}Po and ^{218}Po plateaus as h_1 and h_2, respectively. If $F_1 = F_3$, we have $h_2 = 2h_1$ as observed in both Figs. 6 and 7. If $F_1 > F_3$, we have $h_2 > 2h_1$. The difference $h_2 - 2h_1$ is related to the difference $F_1 - F_3$.

3. Discussion

The approach to tackle the problem of long-term integration measurements of radon progeny can be split into a few sub-problems.

The first one is to devise methods to measure only alpha particles in a specific energy window (i.e., between 6.2 and 7.5 MeV). This will not be a problem for active detectors because discrimination levels can be deployed very accurately. On the contrary, for passive long-term measurements with SSNTDs, the alpha tracks from this group of alpha particles should be recognized and discriminated in the counting phase.

The second one concerns the calibration. Even if we are able to discriminate the tracks that originated from particles in the energy window from 6.2 to 7.5 MeV, we still have to find ways to deduce the ^{214}Po concentration in air from the known specific track density. Experimental calibration is not feasible because it is almost impossible to obtain an atmosphere with ^{214}Po alone and without ^{222}Rn and ^{218}Po. The results given in the present paper were aimed at solving this problem.

The third one deals with determination of the concentrations of the two precursors of ^{214}Po in the radon chain (i.e., ^{218}Po and ^{214}Pb) and determination of the equilibrium factor after knowing the concentration of ^{214}Po. The well-known Jacobi predictive model [7,8] can be useful in this regard. Although the main parameters input into this model, e.g., the decomposition and ventilation rates, have some typical ranges of values, the variations for different situations might still be too large.

One last comment is that the deposition process for radon progeny on the detector surface may disturb the uniformity of distribution of radon progeny in the air in front of the detector, a topic which might be worthy of further investigation in the future.

Acknowledgements

The present research is supported by the CERG Grant CityU1081/01P from the Research Grant Council of Hong Kong (City University of Hong Kong reference number 9040639).

References

[1] International Commission on Radiological Protection (ICRP), Protection against radon-222 at home and at work. ICRP publication 65, Ann. ICRP 23 (2) 1994.
[2] B. Dörschel, E. Piesch, Radiat. Prot. Dosim. 48 (2) (1993) 145.
[3] P. Mozzo, F. Trotti, A. Temporin, M. Lanciai, F. Predicatori, F. Righetti, A. Tacconi, Environ. Int. 1 (Suppl. 22) (1996) S595.
[4] C. Baixeras, K. Amgarou, L.L. Font, C. Domingo, F. Fernandez, Radiat. Meas. 31 (1999) 313.
[5] S.A. Durrani, R.K. Bull, Solid State Nuclear Tract Detectors; Principles, Methods and Applications, Pergamon, Oxford, 1987.
[6] ICRU49 International Commission of Radiation Units and Measurements, Stopping powers and ranges for protons and alpha particles, ICRU Report 49, Bethseda, Maryland, 1993.
[7] W. Jacobi, Health Phys. 22 (1972) 441.
[8] J. Porstendörfer, Radiat. Prot. Dosim. 7 (1/4) (1984) 107.